https://doi.org/10.5194/egusphere-2024-141
Preprint. Discussion started: 15 March 2024

Multitemporal UAV LiDAR detects seasonal heave and subsidence on palsas

Cas Renette[1], Mats Olvmo[1], Sofia Thorsson[1], Björn Holmer[1], Heather Reese[1]

[1]Department of Earth Sciences, University of Gothenburg, Gothenburg, Sweden

Correspondence to: Cas Renette (cas.renette@gvc.gu.se)

https://doi.org/10.5194/egusphere-2024-141
Preprint. Discussion started: 15 March 2024

Abstract

In the context of the accelerating impacts of climate change on permafrost landscapes, we use uncrewed aerial vehicle (UAV) LiDAR technology to investigate seasonal terrain changes in palsas – mounds of frozen peat – since other remote sensing methods have struggled to capture the full dynamics of these landforms. We investigated two palsas (4–5 m in height) in Sweden's largest palsa mire complex, where we performed five field campaigns between September 2022 and September 2023 to track intra-annual frost heave and thaw subsidence. Our approach allowed us to create digital terrain models (DTMs) from high density point clouds (>1,000 points/m²) and analyze elevation changes over time. We found that both palsas heaved on average 0.15 m (and up to 0.30 m) from September to April and subsided back to their height from the previous year, or slightly below, over the course of the following summer. At one of the palsas, we observed notable lateral degradation over the study period in a 300 m² area, with 0.5–2.0 m height loss, likely initiated during the preceding warm and wet summer months. Part of this degradation occurred between September 2022 and April 2023, suggesting that the degradation of these palsas is not limited to the summer months. Our study shows the substantial value of using UAV LiDAR for understanding how permafrost areas are changing. It helps in tracking the ongoing effects of climate change and highlights palsa dynamics that would not be captured by annual measurements alone.

https://doi.org/10.5194/egusphere-2024-141
Preprint. Discussion started: 15 March 2024

1 Introduction

In the face of accelerating climate change, permafrost – defined as ground that remains at or below 0 ◦C for at least two consecutive years (Harris et al., 1988) – is warming at a global scale (Biskaborn et al., 2019). The thickness of the active layer, which is the top layer that thaws and freezes each year (Romanovsky & Osterkamp, 1995), is also increasing at many polar sites (Smith et al., 2022). Palsas, which are peat mounds with a core of perennially frozen soil, are indicative of permafrost presence and serve as particularly vulnerable indicators of climatic changes. They are generally found in subarctic wetlands (Seppälä, 1986), in the discontinuous or sporadic permafrost zone. The climatic space for palsas, typically with a mean annual air temperature between -3 °C and -5 °C and mean annual precipitation <450 mm, according to Luoto et al. (2004a), is projected to disappear in Fennoscandia by the end of the 21st century (Fewster et al., 2022). The degradation of palsas leads to significant changes in this landscape and ecosystem. In recent studies, an increasing lateral degradation rate of palsas is reported (Borge et al., 2017; Mamet et al., 2017; Olvmo et al., 2020), which may have far-reaching consequences for the biodiversity of the subarctic (Luoto, et al., 2004b; Swindles et al., 2015). The transition from an elevated, often dry, palsa bog to a lower lying, wet fen, is associated with an increase in CH_4 and CO_2 emissions (e.g. Łakomiec et al., 2021; Pirk et al., 2023; Swindles et al., 2015; Voigt et al., 2019). Due to the tendency to enhance atmospheric greenhouse gas emissions, degrading palsas therefore not only indicate but can also contribute to climatic change. This climatic feedback mechanism further highlights the need for continued monitoring of these environments. Therefore, palsa mires are a priority habitat of the EU Species and Habitat Directive (*EUNIS -Factsheet for Palsa Mires*, 2013). However, in Sweden only about half (47%) of the total palsa area is situated within some kind of protected area (Backe, 2014).

Permafrost degradation of palsas is indicated by both lateral erosion and vertical subsidence. In addition to this, the elevation of permafrost terrain fluctuates cyclically due to annual freeze-thaw cycles within the active layer (Gruber, 2020; Iwahana et al., 2021), though this has not been explicitly studied on palsas. During fall, freezing of water in the soil and its expansion, in addition to the formation of seasonally segregated ice, can cause heaving of the terrain, while terrain subsidence, caused by the melting of both pore ice and segregated ice, occurs during spring and summer (Fu et al., 2022). The melting of excess

https://doi.org/10.5194/egusphere-2024-141
Preprint. Discussion started: 15 March 2024

ground ice (i.e., ice that is in excess of the total pore volume of the ground in unfrozen conditions; Harris et al., 1988) below the active layer causes longer-term subsidence as result of permafrost thaw. Therefore, thaw-subsidence rates are generally higher in ice-rich than in ice-poor permafrost soils (Gruber, 2020; Zwieback & Meyer, 2021).

While there is growing awareness of the importance of monitoring palsa mires, there is a lack of quantitative measurements of their intra-annual heave and subsidence patterns. de la Barreda-Bautista et al. (2022) used InSAR data to analyze thaw-season subsidence on palsas in northern Sweden but found only sub-cm scale surface level changes. They suggest that this method likely highly underestimated actual displacement rates as a result of spatial averaging. In other recent studies with attempts to quantify both lateral and vertical changes in palsas or peat plateaus, the focus was on multi-year timescales (e.g., Martin et al., 2021; Verdonen et al., 2022) and not on changes occurring within a year. UAV photogrammetry to create digital surface models (DSMs) to study palsas and peat plateaus has been applied more frequently in recent years (de la Barreda-Bautista et al., 2022; Krutskikh et al., 2023; Martin et al., 2021; Verdonen et al., 2023). However, as described in Verdonen (2023), change analysis from DSMs created with UAV photogrammetry is sensitive to relatively minor changes in vegetation and light conditions. Advances in uncrewed aerial vehicles (UAV or drone) in combination with light detection and ranging (LiDAR) technology (Ostrowski et al., 2017) have made it possible to collect accurate, high-resolution (cm-scale) digital terrain models (DTMs) and DSMs. LiDAR sensors can prove advantageous over regular photographic Red-Green-Blue (RGB) imagery, in that LiDAR can penetrate through small gaps in the vegetation allowing creation of DTMs of the underlying ground, whereas RGB cameras require clear sight to the ground surface. LiDAR can also be used in low-light conditions as opposed to RGB imagery, which can be beneficial in the Arctic, where daylight is limited during parts of the year. Another advantage that UAV LiDAR data holds is the absence of need of ground control points (GCPs) due to the potentially low bias of UAV LiDAR data positional errors. This advantage drastically saves time and thus costs on repeated visits (Harder et al., 2020).Therefore, the use of repeat UAV LiDAR scanning is a promising tool for accurate change detection (Curcio et al., 2022; Harder et al., 2020; Jacobs et al., 2021; Lin et al., 2019), but has not yet been widely used to monitor permafrost features.

https://doi.org/10.5194/egusphere-2024-141
Preprint. Discussion started: 15 March 2024

In this study, our objective is to detect and quantify the intra-annual vertical heave and subsidence of two palsas using repeat measurements from UAV LiDAR data. Our findings show seasonal dynamics of the palsas and highlight the substantial potential of UAV LiDAR scanning to study permafrost-mediated landscape changes.

2 Study site: Vissátvuopmi palsa complex

Located near the Finnish border, and just southwest of the Könkämäeno river, Vissátvuopmi is the largest coherent palsa mire complex in Sweden (ca 150 ha of palsa area; Backe, 2014) at N 68°47’50″, E 21°11′30″ (Fig. 1). Surrounded by mountains up to 700 m a.s.l., the valley has several larger lakes, thermokarst features and fens. Two distinct palsas, one ridge-shaped and one dome-shaped (called the “Ridge” and “Dome” palsas from hereon) situated at the foot-slope of a bedrock hill, are the focus of this study and are located between 443 and 452 m a.s.l. (Fig. 1c). In September 2022, the Dome palsa was approximately 170 meters in length and 75 meters in width, with its highest point about 4 meters above the surrounding mire. The Ridge palsa measures about 125 meters in length and 40 meters in width, with its highest point being roughly 5 meters above the adjacent mire terrain. The Dome palsa is taller on its northern and eastern sides, while it flattens out on the western and southern sides. An ATV track runs over the northeastern part of the palsa, which most certainly contributes to amplified degradation of the underlying permafrost by collecting snow and water. The track is visible in aerial photos from 1994 but is absent in the 1963 photos. A natural depression in the center part of the palsa has the same effect and further fragments this palsa. The Ridge palsa is smaller in area but slightly taller. This palsa consists of several crests of similar elevation with depressions in between. The southeastern margin of this palsa is ‘tail-shaped’ and of lower elevation.

https://doi.org/10.5194/egusphere-2024-141
Preprint. Discussion started: 15 March 2024

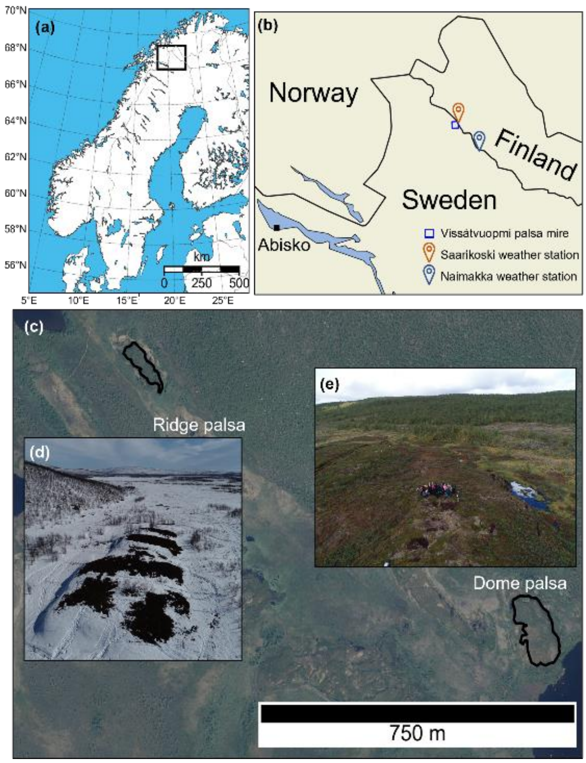

Figure 1. (a,b) Location of the Vissátvuopmi palsa mire complex and used weather stations in Northern Sweden. (c) Orthophoto from 2021 (© Lantmäteriet, 2021) showing a segment of the palsa mire and the location of the two studied palsas. (d) Oblique UAV image highlighting the partly snow-covered Ridge palsa in April 2023. (e) Aerial view of the Dome palsa in September 2023.

The vegetation over the palsa mire complex is characterized by a mosaic of marshes with grasses and sphagnum mosses, wet heaths with willow, and drier areas with subalpine shrub heath. Birch forest occurs primarily on the slopes surrounding the mire, however, birches are also growing within the palsa mire complex. The palsa vegetation consists of dry heath and mesic heath (Andersson et al., 1985) where the field layer is predominantly low-growing *Betula nana* (< 35 cm in mean height), *Empetrum nigrum* ssp *hermaphroditum* and *Rubus chamaemorus.* The bottom layer consists of lichens in higher and drier areas of the palsa, while sphagnum mosses are in lower-lying, wetter areas. At the edges of the palsa, particularly where pools of water have formed, grasses such as *Carex rotundata* and *C. saxatilis* are common, in

https://doi.org/10.5194/egusphere-2024-141
Preprint. Discussion started: 15 March 2024

addition to *Eriophorum russeolum* (Backe, 2014). The ridge palsa has a few birch trees growing on the north and south parts of the palsa.

The Köppen climate type is Subarctic (Dfc) and a weather station operated by the Swedish Meteorological Institute (SMHI) in Naimakka, ca 18 km east of the study site observed a mean annual air temperature of of -1.5 °C and mean annual precipitation was 460 mm in the 1991–2020 standard period. In September 2022, a HOBO weather station was set up in the nearby settlement of Saarikoski, ca. 1.5 km from the study site (see Fig. 1b for location of the two weather stations). Both precipitation and snow depth have been monitored since 2015 at Saarikoski. It is notable that in July 2022 the monthly precipitation was 158 mm, which is more than a third of the mean annual precipitation (Fig. 2).

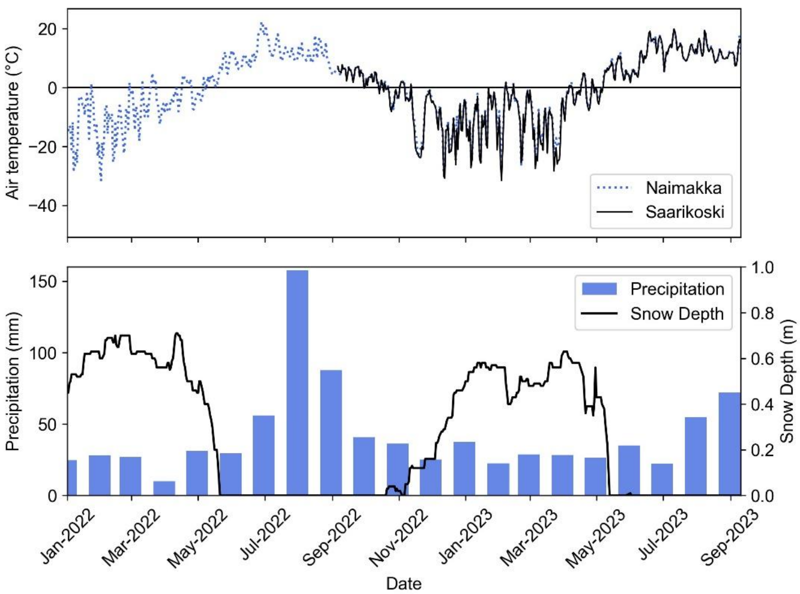

Figure 2. Weather data in the study region between January 2022 and September 2023. (a) Air temperature at ca. 1.5 km (Saarikoski) and at ca. 18 km (Naimakka) from the studied palsas. (b) Monthly precipitation and snow depth observed at Saarikoski.

Based on aerial photo interpretation, Olvmo et al. (2020) reported average areal decay rates of −0.71%a^{-1} and −1.25%a^{-1} in the Dome and Ridge palsa respectively between 1955 and 2016. Additionally, they

https://doi.org/10.5194/egusphere-2024-141
Preprint. Discussion started: 15 March 2024

concluded that palsas in the Vissátvuopmi complex have most likely been in a phase of degradation since the early 20th century.

3 Data and Methods

3.1 LiDAR data acquisition

We used repeat UAV-borne LiDAR scanning to obtain point clouds and create raster-based digital terrain models (DTMs) at a high temporal and spatial resolution. Flights were performed on 4 September 2022, 26 April 2023, 18 June 2023, 19 July 2023, and 7 September 2023. We conducted the scans on these dates to capture the state of the palsas at the end of summer, then observed them when frozen, and continued tracking them throughout the proceeding thawing season. A DJI Matrice 300 RTK UAV was equipped with a YellowScan Mapper (YSM) LiDAR scanner in September 2022 and a YellowScan Mapper + (YSM+) in all following flights (Fig. 3). These are lightweight Livox LiDAR scanners with an Applanix GNSS/INS system. Table 1 shows the properties of the flights and scanner(s). For both of the palsas, a flight with high overlap was done and supported by a second flight with additional orthogonal trajectories. The same flight plans were executed for all five scannings to ensure equal spatial coverage and resolution.

Figure 3. DJI Matrice 300 RTK equipped with the YellowScan Mapper+ in front of the Ridge Palsa.

The April 2023 flights were performed during a period of snowmelt, so that parts of both palsas were snow-free, while other parts remained snow-covered. Consequently, in order to investigate changes in terrain elevation, the snow-free parts needed to be isolated for analysis. For that reason, flights with a second UAV with an RGB camera to create orthomosaics were performed on the same day as the LiDAR scanning.

Table 1 LiDAR scanner and flight parameters of the flying missions. Where values for YellowScan Mapper differ from YellowScan Mapper +, they are shown within parentheses.

Parameter	**Value, YellowScan Mapper + (Mapper)**
Vertical Accuracy (RMSE, m)	0.021 (0.028)
Precision (m)	0.024 (0.032)
Number of returns	3 (2)
Altitude (m.a.g.l.)	60
Velocity (m/s)	8
Overlap (%)	60

Regarding the UAV LiDAR flights, the average flight time was 6 minutes and 49 seconds over the Dome palsa, and slightly shorter over the Ridge palsa at 5 minutes and 13 seconds. Similarly, flights over the Dome palsa yielded a slightly larger coverage area of 53993 m2 compared to the Ridge palsa, which covered an area of 42072 m^2, including part of the surrounding mire and forested mountain. The mean point densities over the Dome palsas were 1327 (YSM) and 1462 (YSM+) points/m^2, and 1201 (YSM) and 1519 (YSM+) points/m^2 at the Ridge palsa. These pulse densities can be regarded as very high, easily allowing the creation of DTMs with high spatial resolution. Terrain features such as surface cracks and blocks of peat are well-identifiable in the LiDAR point cloud data, which emphasizes the high quality of the collected data (Fig. 4).

https://doi.org/10.5194/egusphere-2024-141
Preprint. Discussion started: 15 March 2024

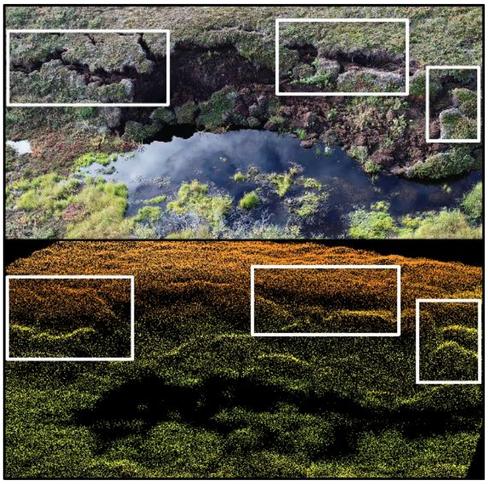

Figure 4. (a) RGB photo of a degrading edge and formation of a thermokarst lake at the Dome palsa, taken with a DJI Phantom 4 UAV in September 2022. (b) Dense UAV LiDAR point cloud taken on the same day with the DJI Matrice 300 RTK equipped with the YellowScan Mapper. Morphological features such as cracks in the surface and individual blocks of peat can clearly be recognized in the point cloud. This section of the palsa reaches a height of ca. 4 meters.

3.2 Point cloud processing and DTM creation

The processing of a LiDAR point cloud requires several steps, including GPS correction, strip adjustment, classification of ground points, and the creation of a DTM raster. The position data captured by the LiDAR system during the flights are postprocessed in PosPac UAV v. 8.2 (*Applanix*, 2023) using PP-RTX for trajectory correction. PP-RTX for UAV uses the Trimble CenterPoint® RTX™ correction service, which computes corrections to satellite orbit and clock data for trajectory correction and positioning, based on a global network of tracking stations. This cloud-based solution gives centimeter-level positioning accuracy without the requirement to set up a local base, which makes PP-RTX particularly advantageous for UAV surveys in remote regions. YellowScan's processing software, CloudStation (*YellowScan*, 2023), is then used for strip adjustment to reduce the relative adjustment error. The point clouds were compared visually for alignment in areas where changes were least likely. Following this, CloudCompare v. 2.12.4 (*GPL software*, 2023) is used to perform the classification of points into ground and non-ground points using the Cloth Simulation Filter (CSF) (Zhang et al., 2016). The CSF method simulates a virtual cloth dropping onto

https://doi.org/10.5194/egusphere-2024-141
Preprint. Discussion started: 15 March 2024

the inverted point cloud. Points that are close to where the cloth settles are classified as ground, while those that are farther away are considered non-ground. The software allows three adjustable parameters for the CSF classification. Several parameter combinations were tested and the best result, based on visual inspection of the resulting point cloud, was achieved with the following parameters: 'Cloth resolution' = 0.1 m (matching the resolution of the created DTMs), 'Max iterations' = 500 and 'Classification threshold' = 0.1 m (controlling the distance of points to be classified as ground), resulting in a detailed ground surface. Only ground points are then used to create the DTM, and in this project a grid cell resolution of 0.1 m was chosen. Since the total thickness of the point cloud along the ground is between ca. 0.10 and 0.30 m, the minimum elevation per grid cell is used during the rasterization in order to ensure that the raster represents the ground elevation. This process is carried out for all five time points, creating a DTM for each scanning and palsa. Finally, the resulting DTMs are used for change detection by subtracting values of one raster from another.

The snow free parts from the April 2023 data were singled out for the computation of heave and subsidence. This was done with georeferenced orthophotos taken on the same day as the LiDAR data, in combination with a hillshade image from the DTM (since the hillshade is smooth where there is snow). For each DTM, the mean elevation of the surrounding mire is computed and subtracted from the DTM, which normalizes the elevation of the palsa into the height above the mire. This simplifies the comparison between the data from the different flights. Since the mire in April was snow-covered, the mire elevation from the closest date (June) was taken for normalizing the April DTM.

4 Results

4.1 Annual terrain changes from UAV LiDAR

Between September 2022 and September 2023, the maximum height difference was 0.03 m, (from 4.21 m to 4.18 m) on the Dome palsa and 0.05 m (4.67 m to 4.62 m) on Ridge palsa (Fig. 5). The largest change in height was detected along the northwest edge of the Dome palsa where an area of ca. 300 m^2 subsided between from 0.5 and 2.0 m. Degradation also occurred along the margins of the Dome palsa, as well as within the ATV track that borders the eastern side of the new 300 m^2 degraded area. The height of the

https://doi.org/10.5194/egusphere-2024-141
Preprint. Discussion started: 15 March 2024

Ridge palsa decreased slightly over the entire landform, with most loss along the margins in the form of lateral degradation.

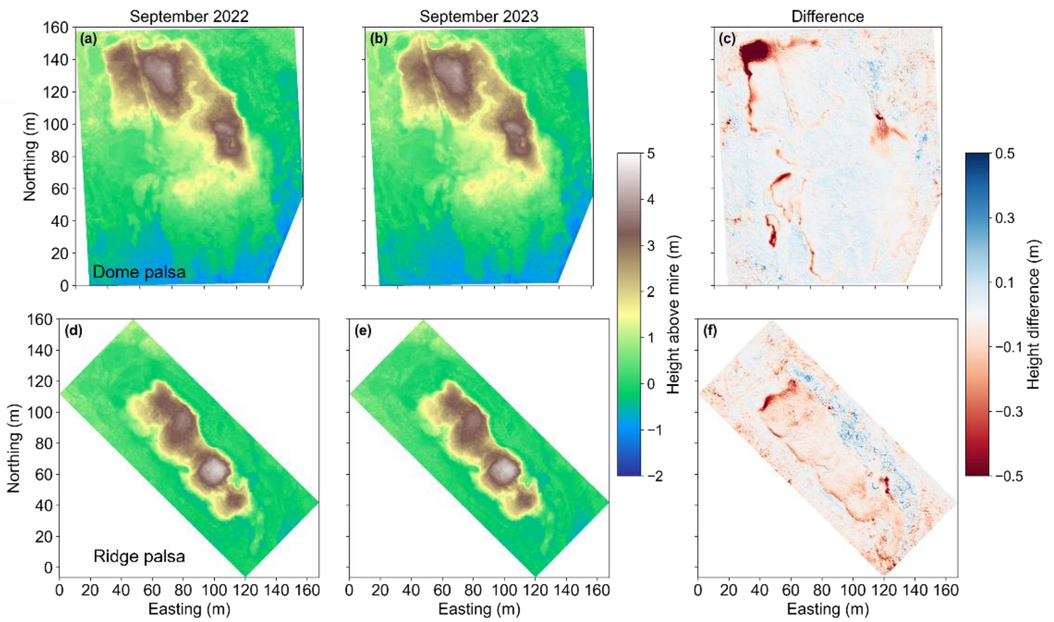

Figure 5. DTMs of the Dome (a,b,c) and Ridge (d,e,f) palsas palsa on UAV LiDAR scans in September 2022 and September 2023. The images highlight the topographical changes over one year.

4.2 Seasonal terrain changes from UAV LiDAR

By comparing each DTM with the following, we observed intra-annual terrain variations, i.e., frost heave and thaw subsidence (Fig. 6). The heterogeneous snow cover that affects this pattern is more clearly visible in Fig. 7c and d.. The snow thickness is up to ca. 2.0 m at the eastern margin of both palsas and 1.0 to 1.5 m in the depressions, while the crests remain snow-free (also see Fig. 1d).. Most interestingly, on these snow-free crests (i.e. Fig. 7f), an elevation increase up to 0.30 m and on average of 0.15 m from September 2022 to April 2023 is observed. Comparing these two closeup parts of the Ridge palsa profile also shows that the subsidence the palsa underwent throughout the year in the depressions was larger than on the crests. Between June and July, both palsas clearly subside all over (Fig. 6c and 6g), on average 0.05 m on

https://doi.org/10.5194/egusphere-2024-141
Preprint. Discussion started: 15 March 2024

the Dome palsa and 0.08 m on the Ridge palsa. Subsidence from July to September is only clear on the Ridge palsa, with 0.05 m on average over the entire palsa.

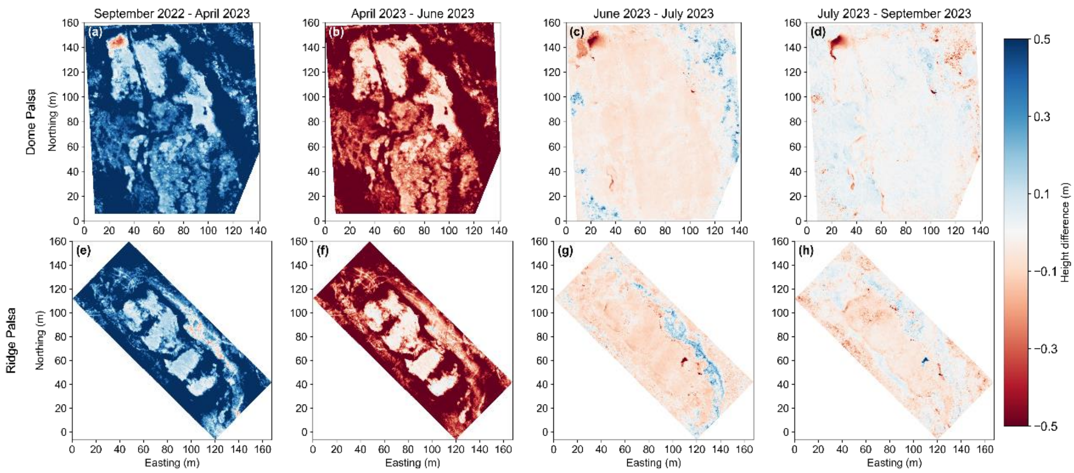

Figure 6. Sequential height difference maps of the Dome (a,b,c,d) and Ridge (e,f,g,h) palsas between each of the five UAV LiDAR DTMs from September 2022 to September 2023. Each panel showcases the topographical changes over successive intervals. Blue colors indicate elevation gains and red colors indicate elevation losses. The snow cover in April is mostly responsible for changes observed to and from those panels.

Even despite the snow cover in April, the northwestern corner of the Dome Palsa shows signs of degradation up to 0.4 m (Fig. 6a), indicating it occurred sometime between September 2022 and April 2023. This degradation remains evident and increases throughout the time series and is visible in Fig. 7c and e, where this area progressively degraded vertically up to 2.0 m between September 2022 and September 2023. Additionally, the ATV track that crosses the Dome palsa shows a deepening of 0.2–0.3 m just over the time period in this study (at ca. 27–29 m in Fig. 7e).

https://doi.org/10.5194/egusphere-2024-141
Preprint. Discussion started: 15 March 2024

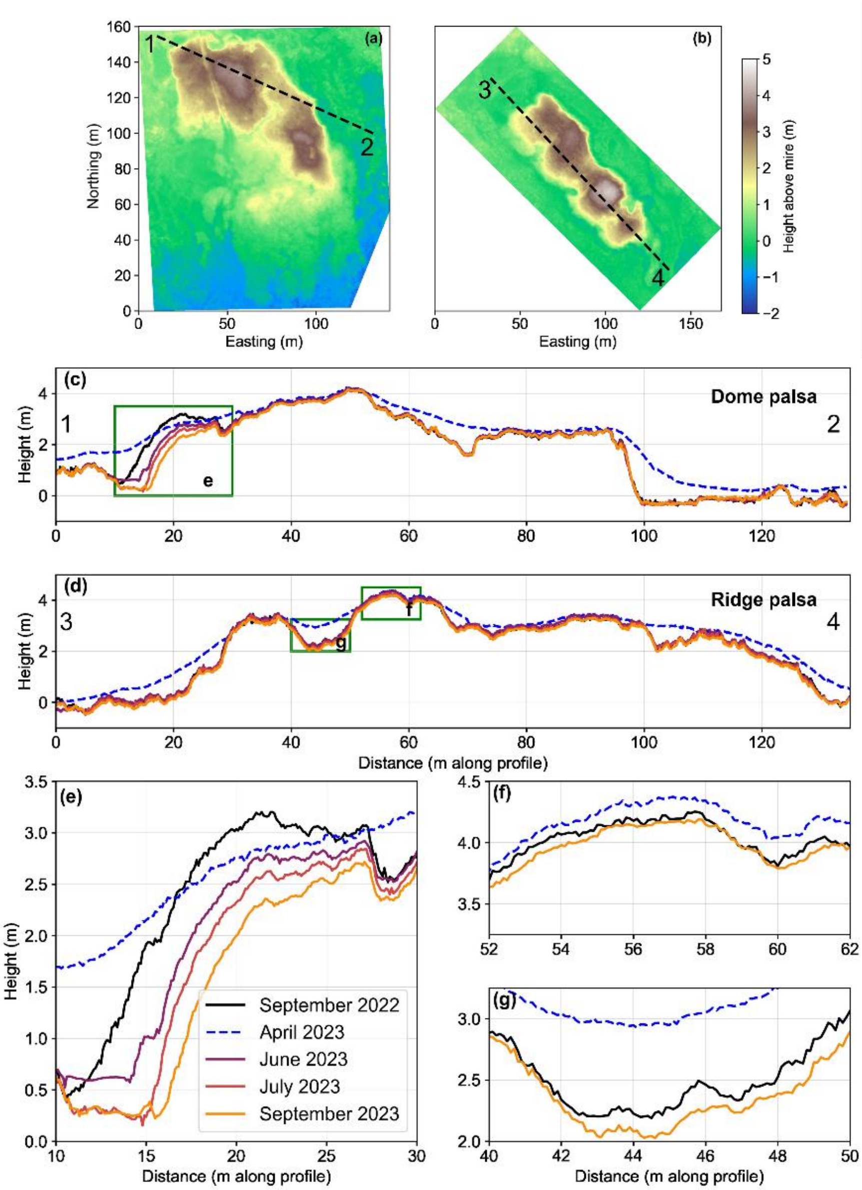

Figure 7. Elevation profiles of the Dome and Ridge palsa based on UAV LiDAR DTMs from September 2022 to September 2023. (a,b) The dashed lines denote the location of the elevation profiles 1-2 and 3-4. (c) and (d) provide a general elevation overview of the transect, while (e), (f), and (g) offer zoomed-in views of specific areas of interest, indicated by the green boxes. The profile from April 2023 is mostly showing the snowpack, although some peaks are snow-free (see also Fig. 1d).

https://doi.org/10.5194/egusphere-2024-141
Preprint. Discussion started: 15 March 2024

The mean height of both palsas increased 0.15 m between September 2022 and April 2023 (Fig. 8). The subsequent flights throughout the summer season show a successive lowering of the palsa height i.e. subsidence. As shown in Fig. 6, the rate of subsidence is highest between the June and July flights. The dome palsa returned to a similar mean height in September 2023 as compared to September 2022, while the ridge palsa subsided to a 0.04 m lower mean height in September 2023 than in September 2022, which is also shown in Fig. 5. Overall, the heave and subsidence pattern is very similar across the two studies palsas.

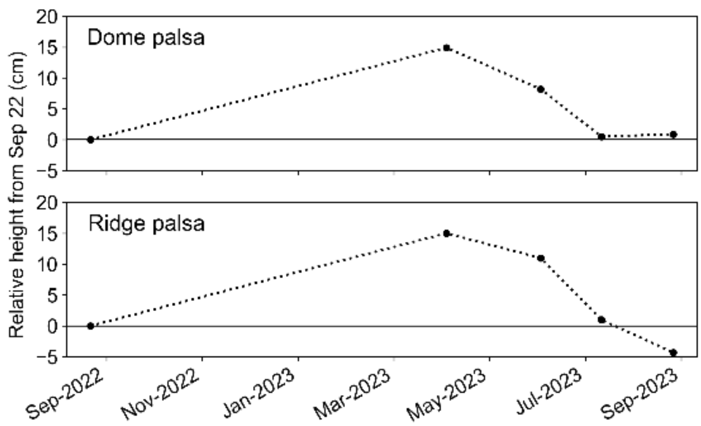

Figure 8. Heave and subsidence on the two studied palsas during the 2022-2023 year. Mean height changes relative to September 2022 are plotted (only for the areas that were completely snow-free in April 2023).

https://doi.org/10.5194/egusphere-2024-141
Preprint. Discussion started: 15 March 2024

5 Discussion

5.1 Intra-annual terrain dynamics on palsas

The objective of this study was to elucidate and quantify the intra-annual dynamics of palsas, and to achieve this, the use of UAV LiDAR proved to be an extremely suitable tool. Analysis of the DTMs indicated that both palsas had frost heave of ca. 0.15 m on average between September and April and subsequent thaw subsidence. This is the first study that covers these dynamics on palsas in such high spatial resolution, although seasonal terrain variability has been investigated in other permafrost environments (Gruber, 2020; Hu et al., 2022; Iwahana et al., 2021; Lin et al., 2019). For example, the heave and subsidence detected in this study are similar to values (0.10 – 0.14 m) observed in the GNSS positioning survey by Iwahana et al. (2021) on an intact tundra site in Alaska after the warm summer of 2019.

The largest rate of subsidence in our study occurred between June and July, which was 0.07 m on the Dome palsa and 0.10 m on the Ridge palsa. Freeze-thaw cycles within the active layer cause frost heave and thaw subsidence, partially due to the density difference between water and ice. However, the average observed heave of 0.15 m cannot be explained alone by this process and requires the formation of seasonal segregation ice (i.e. ice lenses) within the active layer (Fu et al., 2022; Iwahana et al., 2021). Alternatively, processes within the core of the palsa, for example, the infiltration and refreezing along meltwater pathways, might result in seasonal heave and subsidence. To make more conclusive statements about the exact mechanisms, it would be necessary to obtain complementary observations from the interior of these palsas, in the form of soil and ice cores. Taking this step in the future would allow the observed changes in the terrain morphology such as those done here to be better understood in relation to internal palsa dynamics.

The 0.15 m heave is computed on the areas that were snow-free in April and are thus biased towards the crests of the palsas that have a thinner active layer as they have a thinner winter snow cover, which limits the insulation of the ground below. Since the magnitude of the heave and subsidence depends on the thickness of the active layer (Iwahana et al., 2021), the areas with a deeper active layer (i.e., those not included in the computation due to remaining snow in April) are therefore expected to have undergone an even larger increase in height between September 2022 and April 2023. A process other than freeze-thaw

https://doi.org/10.5194/egusphere-2024-141
Preprint. Discussion started: 15 March 2024

dynamics that could have affected the LiDAR measurements is the seasonal oscillation of the peatland surface height due to water table fluctuations, called 'mire breathing' (Kellner & Halldin, 2002; Roulet, 1991). By accounting for the elevational changes in the mire surrounding the palsas, we have corrected for this effect.

We present seasonal patterns at a high spatial resolution over the full spatial extent of two large palsas. While other studies have applied multitemporal LiDAR for detecting permafrost dynamics, they have been terrestrial LiDAR scanning (Anders et al., 2020) rather than UAV-borne LiDAR, or else inter-annual airborne LiDAR (e.g. Douglas et al., 2021; Jones et al., 2015). Anders et al., (2020) performed three TLS measurements over 14 months (June 2015, Aug 2015 and Aug 2016) to observe thaw subsidence of a permafrost area in Northwest Territories, Canada, finding a total change of 1.4 cm; they determined that the TLS measurements were more accurate than those from field-based surveying. Another approach to quantify the effect of seasonal freeze/thaw dynamics on topography is through the use of InSAR remote sensing (de la Barreda-Bautista et al., 2022; Kou et al., 2021; Yanagiya et al., 2023) which can be an effective method to detect the signal of subsidence. Due to its coarser spatial resolution, however, it is likely to underestimate actual heave and subsidence values of smaller isolated features such as palsas.

The time series from this study showed not only the seasonal heave and subsidence patterns, but also revealed a large area of degradation on one of the palsas that happened between September 2022 and April 2023. By comparing the elevation profiles at these two timestamps in the northwest part of the Dome palsa (Fig. 7e), we can see that a drop of up to 0.4 m happened within the autumn and/or winter season, despite the presence of a snow cover in April. It is important to consider that positive air temperatures persisted until the end of October 2022 (Fig. 2), which suggests that the subsidence likely continued into the late autumn period, influenced by prolonged thawing conditions. Whether this entire drop in palsa height occurred solely between the September 2022 campaign and the freeze-up of the entire active layer, or if gravitational processes also contributed after the complete freeze-up, remains uncertain. Regarding the initiation of the degradation at this location, it is likely that it was ongoing earlier in the summer of 2022. Both the air temperatures (>20 °C) and precipitation (158 mm) (both measured at Saarikoski weather station) peaked in July of that year, which could have resulted in a deeply thawed, saturated upper layer of the palsa and initiated a progressive lateral degradation event. The characteristic of this lateral degradation is similar to that described in Martin et al. (2021) as “constant edge degradation”, which they found as the second phase of lateral degradation on peat plateaus following “initial slope adjustment” and preceding “plateau collapse” phases. While both the spatial and temporal scale differ between their and our study, this could indicate that a more widespread collapse or subsidence can follow on the Dome palsa. In order to make more conclusive statements about the reason for this rapid degradation, the monitoring of ground temperatures and knowledge of the internal structure of this palsa is required.

While this described degradation could be just an event, the elevation change of the Dome palsa as a whole from September 2022 to September 2023 was minor. The Ridge palsa, however, did subside on average 0.07 m within one year. The faster degradation on this specific palsa is in line with observations in Olvmo et al. (2020).

5.2 Using UAV LiDAR to monitor permafrost landscapes

The use of UAVs in assessing permafrost landscapes has increased in recent years (de la Barreda-Bautista et al., 2022; Krutskikh et al., 2023; Martin et al., 2021; Siewert & Olofsson, 2020; Sjögersten et al., 2023; Verdonen et al., 2023), although primarily with the use of photogrammetry. Changes in the exterior of permafrost peatlands can be subtle and therefore require the use of highly accurate methods, particularly for vertical subsidence, and when studied over relatively short timescales.

A challenge in permafrost environments, especially palsa mires, is the lack of stable elevation points to be used for ground control points (GCPs). In this study, GCPs were not used, however, , all point clouds were obtained using GNSS, post-processed as described in 3.2, and visually checked for consistency. The elevation profiles (Fig. 7) from the five campaigns are well-aligned and thereby confirm that the positional data are highly accurate. As mentioned by Harder (2020), the use of GCPs is not strictly necessary for UAV LiDAR applications, which significantly contributes to the efficient field visits in harsh Arctic conditions.

In this study, we employed the YellowScan Mapper (YSM) system in September 2022 and the YellowScan Mapper+ (YSM+) in the four campaigns in 2023. The use of an upgraded LiDAR system after the first scanning introduces a potential source of uncertainty in our measurements. However, both systems

https://doi.org/10.5194/egusphere-2024-141
Preprint. Discussion started: 15 March 2024

achieved high point densities (>1,000 points/m²), ensuring detailed surface representation in both datasets despite the difference in the number of recorded returns per pulse. Furthermore, the alignment and positioning of the data were visually verified, showing that the impact of using different systems on our results is minimal. The vertical accuracy of the YSM and YSM+ systems used here have an RMSE of 2.8 and 2.1 cm, respectively. This is a potential error source in the data and changes less than these are within the margin of error. Both systems have a minimum distance of 1 m between registered returns at a flying height of 60 m. This means that all objects on the surface shorter than 1 m in height will be measured by a single return. In this case, to measure the ground elevation underneath vegetation cover requires high point density, which was acquired in this study. By using the minimum elevation per grid cell, the resulting DTM should exclude vegetation heights. In our study, the diffuse cover of *Betula nana* ranged from 0-100% per m² over both palsas, yet the ground could almost always be seen between the sparse branches. Careful consideration of acquisition parameters and algorithms is needed when UAV LiDAR is to be used to create DTMs in areas of extremely dense vegetation cover, or when small grid cell sizes are needed to allow determination of the ground elevation (Kucharczyk et al., 2018).

The ability of LiDAR instruments to measure ground elevation below the vegetation canopy is one of the major advantages that LiDAR has over photogrammetry. Fig. 3 shows, for example, the Ridge palsa with several large birch trees, where terrain analysis can still be done below the canopy. Photogrammetry creates surface models that consist of vegetation height, which is likely to increase over the vegetation season, adding bias to the models. The observed frost heave and subsidence in our study would not have been soundly established with just the use of orthophotos or aerial imagery, due to the potential confusion between vegetation and ground height. A disadvantage when comparing LiDAR and photogrammetric methods is the higher costs of UAV LiDAR scanners at the present time. For that reason alone, when one's objective is to merely compare the perimeter of palsas (e.g, lateral degradation) or other landforms with low-growing vegetation, photogrammetry might still be preferred. While some UAV LiDAR systems can also be integrated with an RGB camera, due to the additional costs, this was not done in this study. The main advantage that this would give is an improved visualization through use of colorized point clouds and could thereby improve the delineation of, for example, snow-covered (or -free) areas.

https://doi.org/10.5194/egusphere-2024-141
Preprint. Discussion started: 15 March 2024

When compared to 'classic' airborne LiDAR surveys, the potential for higher spatial resolution DTMs, ease of planning and lower associated costs do largely favor the use of a UAV when studying permafrost landscapes at least over smaller spatial extents.

6 Conclusions

This study has provided insights into the intra-annual dynamics of palsas through the use of repeat UAV LiDAR measurements, which we highlight as an effective tool for detailed change detection in permafrost landscapes. We present a unique time series of five UAV LiDAR campaigns during a one-year time span on two large palsas in Sweden's largest coherent palsa mire complex. The study revealed seasonal variations in the palsa's topography, with an average frost heave and thaw subsidence of 0.15 m (and up to 0.30 m), with the highest rate of subsidence on the palsas between June and July. The time series also shows a considerable lateral degradation in a 300 m^2 section at one of the palsas of 0.5–2.0 m over the one-year study period. This substantial permafrost degradation occurred between September 2022 and April 2023 which suggests that the degradation palsas is not limited to the summer months. To conclude, the use of repeat UAV LiDAR scanning has proven to be a highly effective tool for capturing detailed measurements of permafrost dynamics, which would not have been observed if only annual measurements had been taken.

https://doi.org/10.5194/egusphere-2024-141
Preprint. Discussion started: 15 March 2024

Data availability

The data presented in this article are stored at 10.5281/zenodo.10497093 (Renette., 2024).

Author contribution

CR and HR designed the study and performed the UAV surveys. HR acquired funding. CR handled data processing, analysis, and figure creation. ST and BH assisted in the setup of the weather station. MO and BH contributed expertise and advice. The manuscript was initially prepared by CR, assisted by HR. All authors reviewed and edited the manuscript draft. All authors approved the final version for submission.

Competing interests

The authors declare that they have no conflict of interest.

Acknowledgements

This work was supported by the Swedish Research Council Formas (grant number 2022-00959), “Threatened subarctic palsa mires: a new integrated approach to map and understand permafrost degradation”. Also, we thank all those that helped with fieldwork and logistics.

https://doi.org/10.5194/egusphere-2024-141
Preprint. Discussion started: 15 March 2024

References

Anders, K., Marx, S., Boike, J., Herfort, B., Wilcox, E. J., Langer, M., Marsh, P., & Höfle, B. (2020). Multitemporal terrestrial laser scanning point clouds for thaw subsidence observation at Arctic permafrost monitoring sites. *Earth Surface Processes and Landforms*, *45*(7), 1589–1600. https://doi.org/10.1002/esp.4833

Andersson, L., Rafstedt, T., & von Sydow, U. (1985). *FJALLENS VEGETATION Norrbottens län: En översikt av Norrbottenfjällens vegetation baserad på vegetationskartering och naturvärdering*. Naturvårdsverket. https://urn.kb.se/resolve?urn=urn:nbn:se:naturvardsverket:diva-7479

Backe, S. (2014). *Kartering av Sveriges palsmyrar* (pp. 1–54) [Text]. https://www.lansstyrelsen.se/norrbotten/om-oss/vara-tjanster/publikationer/2014/kartering-av-sveriges-palsmyrar.html

Biskaborn, B. K., Smith, S. L., Noetzli, J., Matthes, H., Vieira, G., Streletskiy, D. A., Schoeneich, P., Romanovsky, V. E., Lewkowicz, A. G., Abramov, A., Allard, M., Boike, J., Cable, W. L., Christiansen, H. H., Delaloye, R., Diekmann, B., Drozdov, D., Etzelmüller, B., Grosse, G., … Lantuit, H. (2019). Permafrost is warming at a global scale. *Nature Communications*, *10*(1), Article 1. https://doi.org/10.1038/s41467-018-08240-4

Borge, A. F., Westermann, S., Solheim, I., & Etzelmüller, B. (2017). Strong degradation of palsas and peat plateaus in northern Norway during the last 60 years. *The Cryosphere*, *11*(1), 1–16. https://doi.org/10.5194/tc-11-1-2017

CloudCompare (2.12.4). (2023). [Computer software]. GPL software. https://www.danielgm.net/cc/release/

CloudStation (2309.0.0). (2023). [Computer software]. YellowScan. https://www.yellowscan.com/products/cloudstation/

Curcio, A. C., Peralta, G., Aranda, M., & Barbero, L. (2022). Evaluating the Performance of High Spatial Resolution UAV-Photogrammetry and UAV-LiDAR for Salt Marshes: The Cádiz Bay Study Case. *Remote Sensing*, *14*(15), Article 15. https://doi.org/10.3390/rs14153582

de la Barreda-Bautista, B., Boyd, D. S., Ledger, M., Siewert, M. B., Chandler, C., Bradley, A. V., Gee, D., Large, D. J., Olofsson, J., Sowter, A., & Sjögersten, S. (2022). Towards a Monitoring Approach

https://doi.org/10.5194/egusphere-2024-141
Preprint. Discussion started: 15 March 2024

for Understanding Permafrost Degradation and Linked Subsidence in Arctic Peatlands. *Remote Sensing*, *14*(3), Article 3. https://doi.org/10.3390/rs14030444

Douglas, T. A., Hiemstra, C. A., Anderson, J. E., Barbato, R. A., Bjella, K. L., Deeb, E. J., Gelvin, A. B., Nelsen, P. E., Newman, S. D., Saari, S. P., & Wagner, A. M. (2021). Recent degradation of interior Alaska permafrost mapped with ground surveys, geophysics, deep drilling, and repeat airborne lidar. *The Cryosphere*, *15*(8), 3555–3575. https://doi.org/10.5194/tc-15-3555-2021

EUNIS -Factsheet for Palsa mires. (2013). https://eunis.eea.europa.eu/habitats/10155

Fewster, R. E., Morris, P. J., Ivanovic, R. F., Swindles, G. T., Peregon, A. M., & Smith, C. J. (2022). Imminent loss of climate space for permafrost peatlands in Europe and Western Siberia. *Nature Climate Change*, *12*(4), 373–379. https://doi.org/10.1038/s41558-022-01296-7

Fu, Z., Wu, Q., Zhang, W., He, H., & Wang, L. (2022). Water Migration and Segregated Ice Formation in Frozen Ground: Current Advances and Future Perspectives. *Frontiers in Earth Science*, *10*. https://www.frontiersin.org/articles/10.3389/feart.2022.826961

Gruber, S. (2020). Ground subsidence and heave over permafrost: Hourly time series reveal interannual, seasonal and shorter-term movement caused by freezing, thawing and water movement. *The Cryosphere*, *14*(4), 1437–1447. https://doi.org/10.5194/tc-14-1437-2020

Harder, P., Pomeroy, J. W., & Helgason, W. D. (2020). Improving sub-canopy snow depth mapping with unmanned aerial vehicles: Lidar versus structure-from-motion techniques. *The Cryosphere*, *14*(6), 1919–1935. https://doi.org/10.5194/tc-14-1919-2020

Harris, S., French, H., Heginbottom, J., Johnston, G., Ladanyi, B., Sego, D., & Everdingen, R. (1988). *Glossary of Permafrost and Related Ground-Ice Terms*. https://doi.org/10.4224/20386561

Hu, Y., Wang, J., Li, Z., & Peng, J. (2022). Ground surface elevation changes over permafrost areas revealed by multiple GNSS interferometric reflectometry. *Journal of Geodesy*, *96*(8), 56. https://doi.org/10.1007/s00190-022-01646-5

Iwahana, G., Busey, R. C., & Saito, K. (2021). Seasonal and Interannual Ground-Surface Displacement in Intact and Disturbed Tundra along the Dalton Highway on the North Slope, Alaska. *Land*, *10*(1), Article 1. https://doi.org/10.3390/land10010022

https://doi.org/10.5194/egusphere-2024-141
Preprint. Discussion started: 15 March 2024

Jacobs, J. M., Hunsaker, A. G., Sullivan, F. B., Palace, M., Burakowski, E. A., Herrick, C., & Cho, E. (2021). Snow depth mapping with unpiloted aerial system lidar observations: A case study in Durham, New Hampshire, United States. *The Cryosphere*, *15*(3), 1485–1500. https://doi.org/10.5194/tc-15-1485-2021

Jones, B. M., Grosse, G., Arp, C. D., Miller, E., Liu, L., Hayes, D. J., & Larsen, C. F. (2015). Recent Arctic tundra fire initiates widespread thermokarst development. *Scientific Reports*, *5*(1), Article 1. https://doi.org/10.1038/srep15865

Kellner, E., & Halldin, S. (2002). Water budget and surface-layer water storage in a Sphagnum bog in central Sweden. *Hydrological Processes*, *16*(1), 87–103. https://doi.org/10.1002/hyp.286

Kou, X., Liu, X., Zhang, Y., Zhang, Y., Wang, T., & Yan, S. (2021). A Study on the Detection of Deformation of Tuotuohe Area on the Qinghai-Tibet Plateau. *2021 IEEE International Geoscience and Remote Sensing Symposium IGARSS*, 5362–5365. https://doi.org/10.1109/IGARSS47720.2021.9555061

Krutskikh, N., Ryazantsev, P., Ignashov, P., & Kabonen, A. (2023). The Spatial Analysis of Vegetation Cover and Permafrost Degradation for a Subarctic Palsa Mire Based on UAS Photogrammetry and GPR Data in the Kola Peninsula. *Remote Sensing*, *15*, 1896. https://doi.org/10.3390/rs15071896

Kucharczyk, M., Hugenholtz, C. H., & Zou, X. (2018). UAV–LiDAR accuracy in vegetated terrain. *Journal of Unmanned Vehicle Systems*, *6*(4), 212–234. https://doi.org/10.1139/juvs-2017-0030

Lantmäteriet. 2021. GSD-Orthophoto. Available from https://www.lantmateriet.se/sv/Kartor-och-geografisk-information/geodataprodukter/produktlista/ortofoto/ [accessed 1 Nov 2023].

Łakomiec, P., Holst, J., Friborg, T., Crill, P., Rakos, N., Kljun, N., Olsson, P.-O., Eklundh, L., Persson, A., & Rinne, J. (2021). Field-scale CH_4 emission at a subarctic mire with heterogeneous permafrost thaw status. *Biogeosciences*, *18*(20), 5811–5830. https://doi.org/10.5194/bg-18-5811-2021

Lin, Y.-C., Cheng, Y.-T., Zhou, T., Ravi, R., Hasheminasab, S. M., Flatt, J. E., Troy, C., & Habib, A. (2019). Evaluation of UAV LiDAR for Mapping Coastal Environments. *Remote Sensing*, *11*(24), Article 24. https://doi.org/10.3390/rs11242893

https://doi.org/10.5194/egusphere-2024-141
Preprint. Discussion started: 15 March 2024

Luoto, M., Fronzek, S., & Zuidhoff, F. S. (2004a). Spatial modelling of palsa mires in relation to climate in northern Europe. *Earth Surface Processes and Landforms*, *29*(11), 1373–1387. https://doi.org/10.1002/esp.1099

Luoto, M., Heikkinen, R. K., & Carter, T. R. (2004b). Loss of palsa mires in Europe and biological consequences. *Environmental Conservation*, *31*(1), 30–37. https://doi.org/10.1017/S0376892904001018

Mamet, S. D., Chun, K. P., Kershaw, G. G. L., Loranty, M. M., & Peter Kershaw, G. (2017). Recent Increases in Permafrost Thaw Rates and Areal Loss of Palsas in the Western Northwest Territories, Canada: Non-linear Palsa Degradation. *Permafrost and Periglacial Processes*, *28*(4), 619–633. https://doi.org/10.1002/ppp.1951

Martin, L. C. P., Nitzbon, J., Scheer, J., Aas, K. S., Eiken, T., Langer, M., Filhol, S., Etzelmüller, B., & Westermann, S. (2021). Lateral thermokarst patterns in permafrost peat plateaus in northern Norway. *The Cryosphere*, *15*(7), 3423–3442. https://doi.org/10.5194/tc-15-3423-2021

Olvmo, M., Holmer, B., Thorsson, S., Reese, H., & Lindberg, F. (2020). Sub-arctic palsa degradation and the role of climatic drivers in the largest coherent palsa mire complex in Sweden (Vissátvuopmi), 1955–2016. *Scientific Reports*, *10*(1), Article 1. https://doi.org/10.1038/s41598-020-65719-1

Ostrowski, W., Górski, K., Pilarska, M., Salach, A., & Bakuła, K. (2017). Comparison of the laser scanning solutions for the unmanned aerial vehicles. *Archiwum Fotogrametrii, Kartografii i Teledetekcji*, *29*, 101–123. https://doi.org/10.14681/afkit.2017.008

Pirk, N., Aalstad, K., Mannerfelt, E. S., Clayer, F., Wit, H. A. D., Christiansen, C. T., Althuizen, I., Lee, H., & Westermann, S. (2023). *Disaggregating the carbon exchange of degrading permafrost peatlands using Bayesian deep learning* [Preprint]. Preprints. https://doi.org/10.22541/essoar.168394762.23256034/v1

POSPac UAV (8.2). (2023). [Computer software]. Applanix. https://www.applanix.com/products/pospac-uav.html

Renette, C. (2024). Dataset for: "Multitemporal UAV LiDAR detects seasonal heave and subsidence on palsas" (Renette et al., 2024, submitted to The Cryosphere) V1.0, Zenodo [data set], https://10.5281/zenodo.10497093

Romanovsky, V. E., & Osterkamp, T. E. (1995). Interannual variations of the thermal regime of the active layer and near-surface permafrost in northern Alaska. *Permafrost and Periglacial Processes*, *6*(4), 313–335. https://doi.org/10.1002/ppp.3430060404

Roulet, N. T. (1991). Surface Level and Water Table Fluctuations in a Subarctic Fen. *Arctic and Alpine Research*, *23*(3), 303–310. https://doi.org/10.2307/1551608

Seppälä, M. (1986). The Origin of Palsas. *Geografiska Annaler: Series A, Physical Geography*, *68*(3), 141–147. https://doi.org/10.1080/04353676.1986.11880167

Siewert, M. B., & Olofsson, J. (2020). Scale-dependency of Arctic ecosystem properties revealed by UAV. *Environmental Research Letters*, *15*(9), 094030. https://doi.org/10.1088/1748-9326/aba20b

Sjögersten, S., Ledger, M., Siewert, M., De la Barreda-Bautista, B., Sowter, A., Gee, D., Foody, G., & Boyd, D. (2023). Optical and radar Earth observation data for upscaling methane emissions linked to permafrost degradation in sub-Arctic peatlands in northern Sweden. *Biogeosciences*, *20*, 4221–4239. https://doi.org/10.5194/bg-20-4221-2023

Smith, S. L., O'Neill, H. B., Isaksen, K., Noetzli, J., & Romanovsky, V. E. (2022). The changing thermal state of permafrost. *Nature Reviews Earth & Environment*, *3*(1), Article 1. https://doi.org/10.1038/s43017-021-00240-1

Swindles, G. T., Morris, P. J., Mullan, D., Watson, E. J., Turner, T. E., Roland, T. P., Amesbury, M. J., Kokfelt, U., Schoning, K., Pratte, S., Gallego-Sala, A., Charman, D. J., Sanderson, N., Garneau, M., Carrivick, J. L., Woulds, C., Holden, J., Parry, L., & Galloway, J. M. (2015). The long-term fate of permafrost peatlands under rapid climate warming. *Scientific Reports*, *5*(1), Article 1. https://doi.org/10.1038/srep17951

Verdonen, M., Störmer, A., Lotsari, E., Korpelainen, P., Burkhard, B., Colpaert, A., & Kumpula, T. (2023). Permafrost degradation at two monitored palsa mires in north-west Finland. *The Cryosphere*, *17*(5), 1803–1819. https://doi.org/10.5194/tc-17-1803-2023

Voigt, C., Marushchak, M. E., Mastepanov, M., Lamprecht, R. E., Christensen, T. R., Dorodnikov, M., Jackowicz-Korczyński, M., Lindgren, A., Lohila, A., Nykänen, H., Oinonen, M., Oksanen, T., Palonen, V., Treat, C. C., Martikainen, P. J., & Biasi, C. (2019). Ecosystem carbon response of an Arctic peatland to simulated permafrost thaw. *Global Change Biology*, *25*(5), 1746–1764. https://doi.org/10.1111/gcb.14574

Yanagiya, K., Furuya, M., Danilov, P., & Iwahana, G. (2023). Transient Freeze-Thaw Deformation Responses to the 2018 and 2019 Fires Near Batagaika Megaslump, Northeast Siberia. *Journal of Geophysical Research: Earth Surface*, *128*. https://doi.org/10.1029/2022JF006817

Zhang, W., Qi, J., Wan, P., Wang, H., Xie, D., Wang, X., & Yan, G. (2016). An Easy-to-Use Airborne LiDAR Data Filtering Method Based on Cloth Simulation. *Remote Sensing*, *8*(6), Article 6. https://doi.org/10.3390/rs8060501

Zwieback, S., & Meyer, F. J. (2021). Top-of-permafrost ground ice indicated by remotely sensed late-season subsidence. *The Cryosphere*, *15*(4), 2041–2055. https://doi.org/10.5194/tc-15-2041-2021